The Thirteenth International Symposium on Artificial Life and Robotics 2008(AROB 13th '08),
B-Con Plaza, Beppu, Oita, Japan, January 31-February 2, 2008

Orbit Systematics in Anisotropic Kepler Problem

Tokuzo Shimada, Kazuhiro Kubo
Department of physics, School of Science and Technology, Meiji University
1-1-1 Higashimita, Tama, Kawasaki, Kanagawa 214-8571

Abstract

We revisit the Anisotropic Kepler Problem (AKP), which concerns with trajectories of an electron with anisotropic mass term in a Coulomb field. This is one of the most fundamental fields in Quantum Chaos. Nowadays various quantum systems are challenging us. Classical theories of these have chaos, while quantum theories have developed from integrable cases and may need to be reformulated. AKP then serves as a suitable testing ground for quantum chaos. Here we shed some light on the systematics of the trajectories using ample figures from an extensive numerical analysis. In particular, the role of hyperbolic singularities is illuminated. List of critical trajectories are given in page 3. We comment on the validity of approximations in an analytic formulation.

Keywords: quantum chaos, anisotropic Kepler problem, collision trajectory, hyperbolic singularity.

1 Introduction

We revisit the AKP and shed some light on the systematics of orbits from extensive numerical calculations. In this field the pioneering paper by Martin Gutzwiller in 1977 is prominent [1]. By lucid analytic consideration important features of orbits in the theory are revealed. Especially it proves why there exists an orbit which corresponds to a given Bernoulli code of the Poincaré section. Unfortunately, however, the paper has only one figure concerning orbits, namely the vector field for the orbit. This vector field is based on an approximation which is valid only when the point particle is extremely near the origin (the Coulomb singularity point). However, important orbits, collision orbits, pass nearby a hyperbolic singularity point and there, at the very crucial point, the approximation becomes invalid. Therefore, one must be extremely careful in deducing physical predictions from the vector field. ([1] is collect.) We carefully check the approximations adopted in various places in one hand and on the other hand we describe the systematics of the orbits in AKP which we have caught in an extensive numerical study. In AKP our familiar picture for Keplerian orbits must be abandoned - the first three orbits in Fig. 1 are (a) a symmetric periodic, (b) an asymmetric periodic, (c) a chaotic orbit in AKP respectively.

Nowadays various new quantum systems, electrons in a nano size billiard [3], laser-trapped atoms [4], blight solitons in BE condensates [5] are challenging us. As in Einstein's criticism [6], present quantum mechanics may have to be reformulated since they have chaos in their classical regime. Feynman's path integral uses orbits in quantization, and comparison with experiments are easy. A most remarkable is the Gutzwiller's trace formula [2], which may also offer a key to solve the Riemann Hypothesis. Therefore the classical orbits are important for the quantum physics. AKP serves as a test bench of the theory – to some extent tractable analytically and yet has a hard chaos classically.

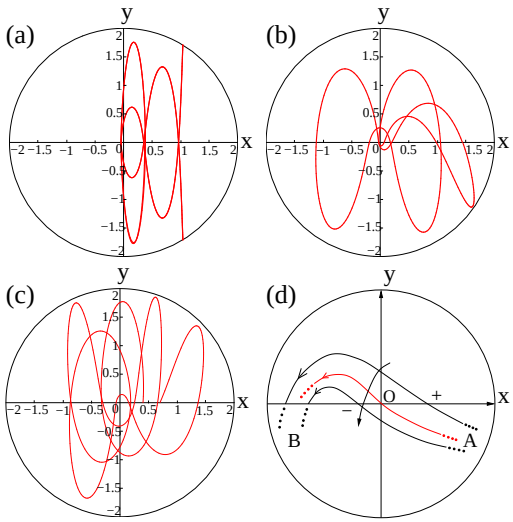

Fig. 1. AKP orbits and the mechanism of Bernoulli code change.

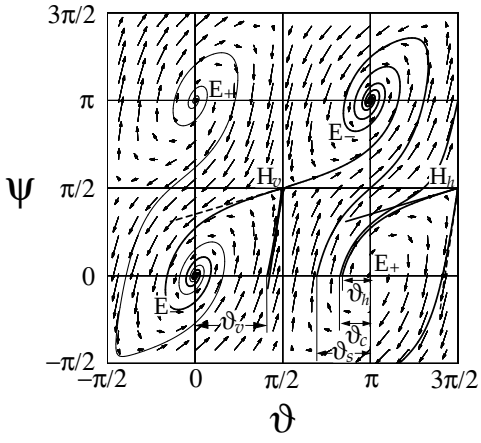

Fig. 2. The vector field (4) at the $\mathcal{A}$ approx.

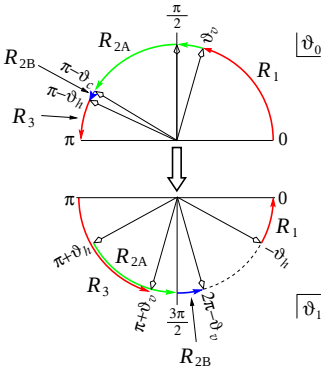

Fig. 3.

Region	ϑ_0	ϑ_1	(U_0, U_1)	$(a_0\ a_1)$	
1	$0 < \vartheta_0 < \vartheta_v$	$\vartheta_h < \vartheta_1 < 0$	(B, B)	$(++)$	a
	$\vartheta_0 \approx \vartheta_v$	Comming out into non-$\mathcal{A}$ via collision.			a',b'
2A	$\vartheta_v < \vartheta_0 < \frac{}{2}$	$\pi + \vartheta_h < \vartheta_1 < \frac{3}{2}\pi$	$(B,\ B)$		b
	ϑ_0 exceeds $\frac{}{2}$	$\rightsquigarrow$	$[U_0 : B \to 0 \to\ B]$		b→c→d
2A	$\frac{}{2} < \vartheta_0 < \vartheta_c$	$\pi + \vartheta_h < \vartheta_1 < \frac{3}{2}\pi$	$(\ B,\ B)$	$(+\ )$	d
	ϑ_0 exceeds ϑ_c	$\rightarrow$ ϑ_1 exceeds $\frac{3}{2}\pi$	$\rightsquigarrow [U_1 :\ B \to 0 \to B]$		d→e→f
2B	$\vartheta_c < \vartheta_0 < \vartheta_h$	$\frac{3}{2}\pi < \vartheta_1 < 2\pi + \vartheta_h$	$(\ B, B)$		f
	$\vartheta_0 \approx \vartheta_h$	Going into the $\mathcal{A}$ region.			
3	$\vartheta_h < \vartheta_0 < \pi$	$\pi < \vartheta_1 < \pi + \vartheta_v$	$(\ B,\ B)$	$(++)$	g

Table 1.

2 Kinematics and Orbits in AKP

The AKP Hamiltonian is

$$H = \frac{u^2}{2} + \frac{v^2}{2} \quad \frac{1}{(x^2+y^2)^{1\ 2}} \tag{1}$$

with $\ > 1$, $\ = 1/\ $. On the Poincaré surface of section $(y = 0)$, $H = \ 1/2$ gives $|x| \ \ 2/(1+u^2/\ )$, $|u| < \infty$.

By an area preserving transformation

$$X = x\left(1 + u^2/\ \right), \quad U = \sqrt{\ }\arctan\left(u/\sqrt{\ }\right), \tag{2}$$

we can map it to a rectangular region $|X| \leqslant 2$, $|U| \leqslant B$. Here $B \equiv \sqrt{\ }\pi/2$ and this abbreviation will be used throughout this paper. It is important to pay attention to the trajectories around the origin in the xy plane. We use polar coordinates for both position and momentum; $(u, v) = \sqrt{\ }e\ (\cos\vartheta, \sin\vartheta)$ and $(x, y) = r(\cos\psi, \sin\psi)$. $H = e^2\ /2 \quad 1/r \equiv \ 1/2$ gives

$$r = 2/(1 + e^2\ ), \quad 0 < r < 2, \qquad \infty < \chi < \infty \tag{3}$$

The Hamilton equation is now

$$\frac{d\vartheta}{d\chi} = \frac{\sqrt{\ }\cos\vartheta\sin\psi \quad \sqrt{\ }\sin\vartheta\cos\psi}{\sqrt{\ }\cos\vartheta\cos\psi + \sqrt{\ }\sin\vartheta\sin\psi},$$
$$\frac{d\psi}{d\chi} = \frac{2}{1+e^{-2}} \quad \frac{\sqrt{\ }\cos\vartheta\sin\psi \quad \sqrt{\ }\sin\vartheta\cos\psi}{\sqrt{\ }\cos\vartheta\cos\psi + \sqrt{\ }\sin\vartheta\sin\psi}, \tag{4}$$

where $d\chi/dt$ equation is used to trade t to χ. Very close to the origin, $\chi \to \infty$, then (4) becomes autonomous. Let us call this as $\mathcal{A}$ approximation and the region $r \approx 0$ (very large χ) as $\mathcal{A}$ region.

The points on the $\vartheta\psi$ plane where the vector field in (4) has a zero component are called singular points. There are two types of singularities; (a) $\sin\vartheta = \sin\psi = 0$ (elliptic singularities), (b) $\cos\vartheta = \cos\psi = 0$ (hyperbolic singularities). In general, trajectory starting in $\mathcal{A}$ remains in $\mathcal{A}$ in a finite time. But, if the trajectory passes through the singularity, then χ may be arbitrary small and the trajectory comes out from the origin in the xy plane.

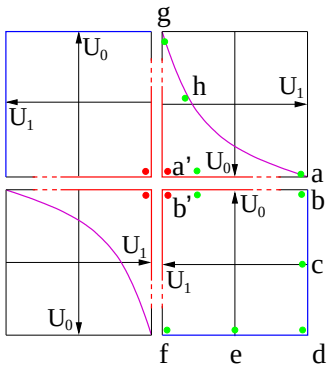

Fig. 4. Type (a_0, a_1)=(++),(+), ( ),(+) arcs are shown in $U_0\ 1$ B in the 1st to the 4th quadrant. Virial R is maximum at four points at the center. Collision arcs locate along the inner boundaries (e.g. a , b). Arcs along the x locate along curves in the 1st and the 3rd quadrants (e.g. h).

2.1 Classification of arcs

In the ergodicity analysis it is useful to introduce an arc $(U_0, U_1)_{(a_0\ a_1)}$, which start at a Poincaré section with U_0 and comes back to it with U_1 and suffixes (a_0, a_1) denote signs of x_0 and x_1 at the crossings. We survey here which kind of an arc will follow when we start it at various ϑ_0 at a given large χ_0 i.e. from $\mathcal{A}$ region. ($\psi_0 = 0$ is chosen for $y_0 = 0$.) There are four characteristic angles. Denoting $\vartheta \ \equiv \pi \ \ \vartheta$, (i) the arc with $\vartheta_0 = \vartheta_v$ passes through H_v, (ii) the arc with $\vartheta_0 = \vartheta_s$ produces an arc symmetric wrt $(\pi,\ \pi/2)$, (iii) the arc with $\vartheta_0 = \vartheta_c$ reaches $(3\pi/2,\ \pi)$, (iv) the arc with $\vartheta_0 = \vartheta_h$ passes H_h [1]. See Fig. 2.

Arcs starting from $\mathcal{A}$ region, so they stay in the $\mathcal{A}$ region till the next crossing of x axis. As they are in the $\mathcal{A}$ region we find

$$X \ \approx \ 2\cos\psi\cos^2\vartheta \tag{5}$$
$$U \ \approx \ \sqrt{\ }\,\mathrm{sign}\,(\cos\vartheta)\left(\frac{\pi}{2} \quad \frac{1}{e\ \ |\cos\vartheta|}\right). \tag{6}$$

Therefore, the arc is of type $(a_0, a_1) = (+, \ \ )$ depending whether $\psi_1 = 0$ or π. The $(U_0, U_1) \approx (\ B, \ \ B)$, depending on the signs of $\cos(\vartheta_0)$ and $\cos(\vartheta_1)$.

The vector field determines ϑ_1 and ψ_1 from ϑ_0 (at fixed χ_0) in a way shown in Fig. 3 and Table 1. The interval $0 < \vartheta_0 < \pi$ divides into three subintervals $\psi_1 = (0,\ \pi,\ 0)$ and $(\mathrm{R}_1, \mathrm{R}_2, \mathrm{R}_3)$. and, by (5), the

[1] These are named by Gutzwiller [1].

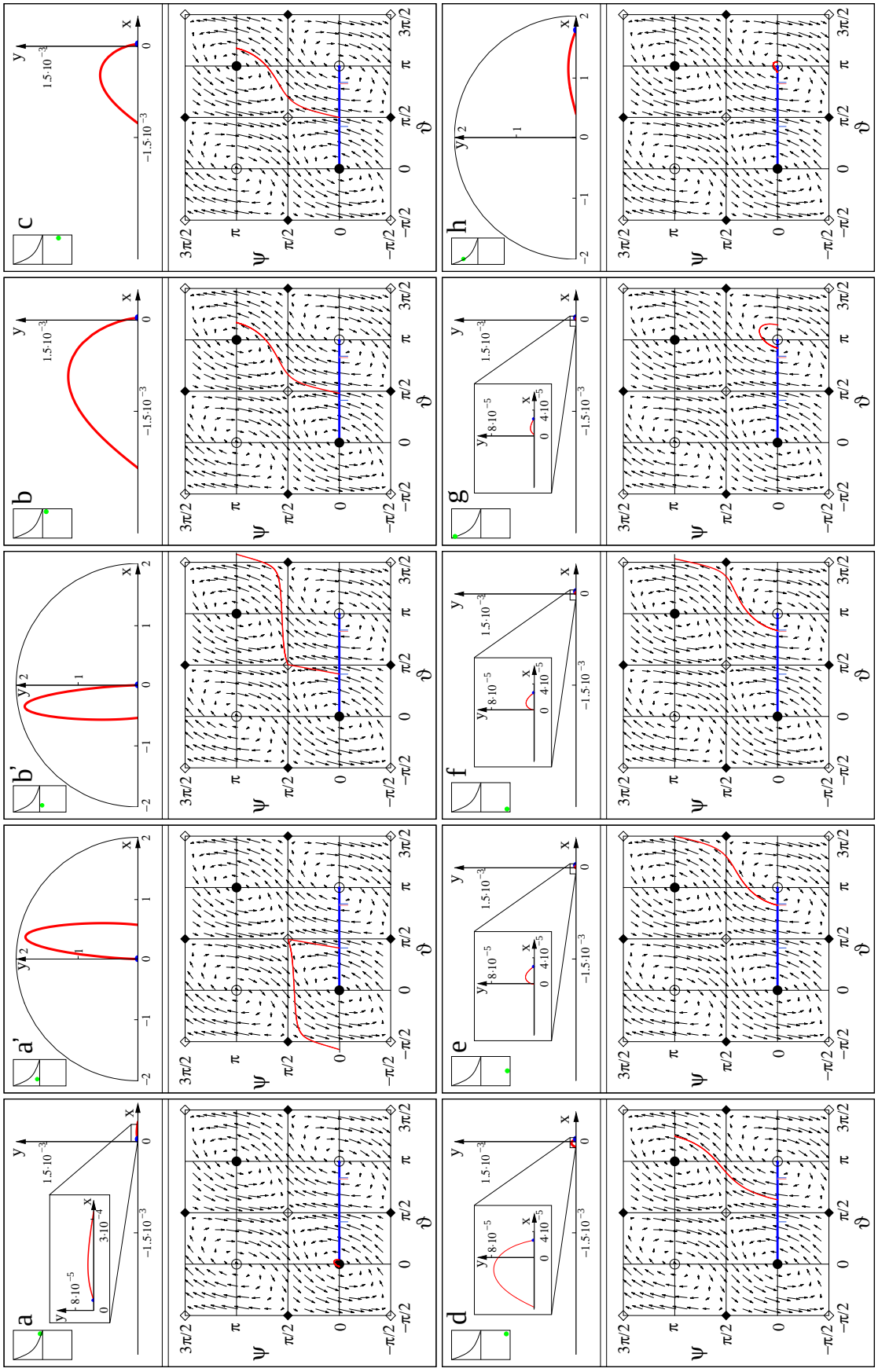

Fig. 5: Typical arcs in the increasing order of ϑ_0, ($\chi_0 = 7$) and their positions on (U_0, U_1) domains. Upper: profiles on the xy plane. Arcs a', b', h come out in null $\mathcal{A}$ region and shown without magnification. Arcs a, b , g are magnified by 10^3 (and insets with further magnification of factor 20 are included except for b, c. Lower: profiles on the $\vartheta\psi$. Vector fields at $\mathcal{A}$ approximation (Fig. (2) is superimposed. Circles : elliptic singularities (white for sources and black for sinks), diamonds : hyperbolic singularities (white for H_v and black for H_h). Three ticks for ϑ_v, ϑ_c, ϑ_h in increasing order of ϑ_0.

arc is of type $(++), (+\ \ ), (++)$ respectively (See the third column of Table 1). To find (U_0, U_1) by (6), we must pay attention that $\vartheta_0 = \pi/2$ and $\vartheta_1 = 3\pi/2$ (that is $\vartheta_0 = \vartheta_c$) give additional criticality. This issue is accounted for in Fig. 3. When ϑ_0 passes through $\pi/2$, U_0 changes as $B \to 0 \to \ \ B$ with $U_1 \approx \ \ B$ and the arc moves rapidly on the boundary of the square domain (for arc $(+\ \ )$) as denoted [b $\to$ c $\to$ d] in Fig. 4. Now the map $\vartheta_0 \to (U_0, U_1)_{(a_0\ a_1)}$ is completed analytically for the arcs in $\mathcal{A}$ region [1].

Above analysis in turn reveals the importance of collision trajectories, which starts either with $\vartheta_0 \approx \vartheta_v$ or $\vartheta_0 \approx \vartheta_h$. Examples of these are a' and b' in Table 1. Fig. 4 are organized so that a' and b' locate face to face. In this organization all arcs in $\mathcal{A}$ locate along the outer boundaries of the domain.

2.2 Profiles of Arcs

In Fig. 5 we visualize our arcs a to g both in xy plane and in $\vartheta\psi$ plane. All are evaluated with high accuracy and large deviation from the vector field as seen around singular points indicate $\mathcal{A}$ approximation is invalid there. Below we discuss collision trajectories a', b', and another null-$\mathcal{A}$ arc, h.

a′ : Starting with $\vartheta_0 = 0.998\vartheta_v$ this comes close to the hyperbolic singularity $H_v(\pi/2, \pi/2)$ and then turns to the left, and eventually comes back to $\psi = 0$ (type $(+,+)$). A large deviation from $\mathcal{A}$ approximation occurs around and after H_v. At $\mathcal{A}$ approximation $\ \ \vartheta_h < \vartheta_1 < 0$, but a precise calculation shows $\vartheta_1 < \ \ \vartheta_h$. Due to the rapid χ decrease around H_v, the orbit in the xy plane comes out from the origin. It moves along y axis because $\psi \approx \pi/2$, $\vartheta \approx \pi/2$ around H_v. Initially the orbit has $u_0 > 0$, but it turns into $u_1 < 0$. Therefore the arc locates in lower left corner in the square domain $|U_{0\,1}| \quad B$ for arc $(++)$.

b′ : This starts with $\vartheta_0 = 1.002\vartheta_v$. This makes a pair with a'; it turnes to the right (rather than left) around H_v and reaches $\psi_1 = \pi$ (arc $(+\ \ )$). This locates face to face with a' in Fig. 4

h : This starts in null-$\mathcal{A}$ region and moves around the elliptic singularity $E(\pi, 0)$. Hence it moves along x axis.

3 Collision Trajectory

Collision trajectory is important because it introduces the ergodicity in the AKP system. In terms of symbolic dynamics a trajectory is coded by the Bernoulli sequence $(a_0, a_1, a_2, \ \ )$ and, as seen in Fig. 1(d), the change in the code may only occur via a collision with the origin.

Let us investigate the collision trajectory ($\vartheta_0 = 0.999\vartheta_v$ at $\chi_0 = 7$) in Fig. 6. The hyperbolic singularity $H_v(\pi/2, \pi/2)$ plays a rolê of a *catapult* to emitt the particle from the origin. Since χ_0 is very large, the trajectory firstly starts very near the origin of the xy plane ($r_0 \approx 1.6 \quad 10^{-6}$) with enormous momentum. The particle moves rapidly on the $\vartheta\psi$ plane (ticks on the trajectory indicate every factor of ten increase of t) and it comes already within $\Delta\vartheta \approx 0.005$ of $H_v(\pi/2, \pi/2)$ at about $t = 10^{-6}$. The particle is now *launched in the catapult*. Till then χ remains large ($\chi \approx 5$), and the particle is still very near to the origin ($r = 10^{-4}$). Now the second step starts

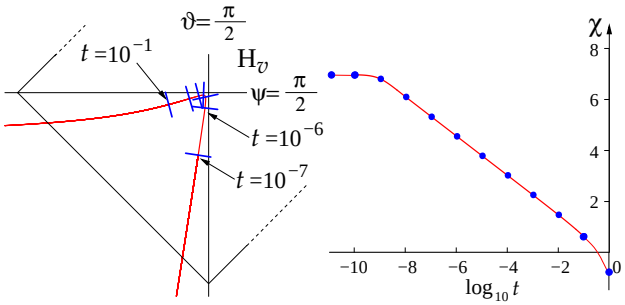

Fig. 6. Frame represents tiny white diamond around H_v in Fig. 5.

under the influence of H_v. The trajectory developes on $\vartheta\psi$ plane much slower, turning around H_v gradually with factor 10^5 increase of time (t from 10^{-6} to 10^{-1}). Correspondingly χ decreases rapidly (from 7 to 1), and the particle is now emitted into the null $\mathcal{A}$ region ($r \approx 0.1$).

In conclusion we hope our results in this paper, in particular (i) a summary of systematics of orbits, Table 1, (ii) List of orbits in Fig. 5, (iii) orbits analysis near a hyperbolic singularity in Fig. 6 may supplement the article [1] and serve useful data for AKP.

References

[1] M. C. Gutzwiller, J. Math. Phys. **18**, 806 (1977).

[2] M. C. Gutzwiller, J. Math. Phys. **12**, 343 (1971).

[3] For instance, R. P. Taylor, Phys. Rev. Lett. **78**, 1952, 1997; Phys. Rev. **B73**, 235321 (2006).

[4] For instance, C. Monroe et al., Phys. Rev. Lett.**65**, 1571, (1990). Also, M. Tachikawa, T. Shimada, H. Otajima, *Experimental Study of Quantum Chaos using Atomic Optics*, supported by Grant-in-Aid for Scientific Research 2004-2006.

[5] S. L. Cornish, S. T. Thompson and C. E. Wieman, Phys.Rev. Lett. **96**, 170401 (2006)
A. D. Martin, C. S. Adams, S. A. Gardiner, Phys. Rev. Lett. **98**, 020402 (2007).

[6] A. Einstein, Verh. Dtsch. Phys. Ges. **19**, 82, 1917.